

# Suppression of Cross-Band Scattering in Multiband Antenna Arrays

Hai-Han Sun<sup>✉</sup>, Graduate Student Member, IEEE, Can Ding<sup>✉</sup>, Member, IEEE, He Zhu<sup>✉</sup>, Member, IEEE,  
Bevan Jones, Life Member, IEEE, and Y. Jay Guo<sup>✉</sup>, Fellow, IEEE

**Abstract**—This paper presents a novel method of suppressing cross-band scattering in dual-band dual-polarized antenna arrays. The method involves introducing chokes into low-band (LB) elements to suppress high-band (HB) scattering currents. The experimental results show that by inserting LB-pass HB-stop chokes into LB radiators, suppression of induced HB currents on the LB elements is achieved. This greatly reduces the pattern distortion of the HB array caused by the presence of LB elements. The array considered is configured as two columns of HB antennas operating from 1.71 to 2.28 GHz interleaved with a single column of LB antennas operating from 0.82 to 1.0 GHz. The realized array with choked LB element has stable and symmetrical radiation in both HB and LB.

**Index Terms**—Dual-band antenna arrays, interleaved arrays, pattern distortion, scattering suppression.

## I. INTRODUCTION

THE ever-increasing demand on wireless communications and sensing, has led to growing interest in multiband antennas to simultaneously support different services. The arrays for different bands usually share a common ground plane and radome, and elements of different bands are often interleaved to save space. However, the close proximity of the elements causes distortion of radiation pattern due to the scattering of the signals of one band by the antenna elements operating in another band [1]. Since low-band (LB) antenna elements are typically larger than high-band (HB) ones, suppression of the scattering of HB signals from LB elements can significantly improve the system performance.

In this paper, we consider a multiband 3G and 4G base station antenna (BSA) array as a typical example. Such antennas need at least an LB antenna array operating from 0.69 to 0.96 GHz, and an HB antenna array operating from 1.71 to 2.69 GHz. The LB and HB antenna arrays share the same area to minimize the space rental cost. As the HB frequencies are almost one octave above the LB frequencies, the HB and LB elements are usually interleaved in a uniform way where the spacing of HB elements is half that of the LB elements. Common arrangements of HB and LB dual-polarized elements in arrays are shown in Fig. 1. In Fig. 1(a),

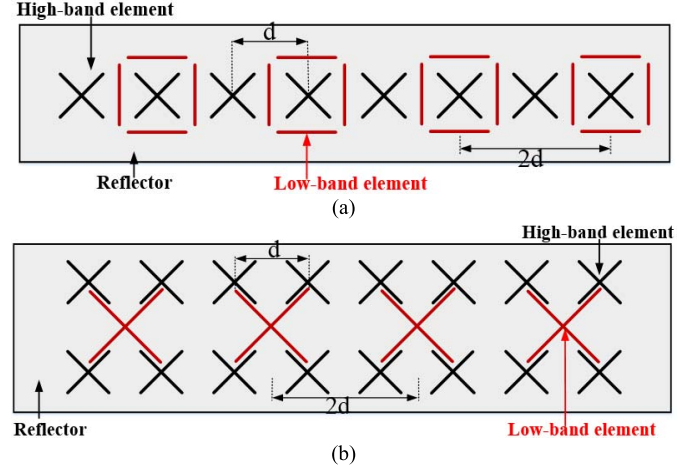


Fig. 1. Dual-band dual-polarized BSA array configurations with (a) embedded scheme and (b) interleaved scheme.

every second HB element is embedded in a physically larger LB element, which is referred as “embedded scheme”. A number of dual-band dual-polarized arrays with this scheme are described in [2]–[9]. Different shapes of metal walls are added to control the radiation patterns and improve isolation between LB and HB elements. An alternative configuration is the “interleaved scheme” shown in Fig. 1(b), where one LB column is located midway between the two HB columns. This configuration is common in practice as it provides multiple-input and multiple-output (MIMO) capability in HB and LB in a minimum width package [10]. A problem with this configuration is that due to the proximity of the HB and LB elements and the electrically large dimension of the LB element at HB, HB currents are induced on the LB element, which radiate unwanted signal at HB. This scattered signal causes a major distortion of the HB radiation pattern.

The reverse effect of distortion of the LB pattern due to the presence of the HB elements can occur if the HB elements have a resonance within or adjacent to the LB. It normally occurs in a relatively narrow band around the LB resonance but can have a serious effect on the LB azimuth pattern. However, this generally can be corrected by moving the resonance out of the LB of interest. This issue is not considered in this paper.

One method of minimizing scattering where closely spaced radiators operate at different frequencies makes use of mantle cloaking techniques, as described in [1] and [11]–[15].

Manuscript received August 16, 2018; revised November 23, 2018; accepted January 1, 2019. Date of publication January 10, 2019; date of current version April 5, 2019. This work was supported by the Australian Research Council under Grant DP160102219. (*Corresponding author:* Can Ding.)

The authors are with the Global Big Data Technologies Centre, University of Technology Sydney, Ultimo, NSW 2007, Australia (e-mail: haihan.sun199403@gmail.com; can.ding.1989@gmail.com).

Color versions of one or more of the figures in this paper are available online at <http://ieeexplore.ieee.org>.

Digital Object Identifier 10.1109/TAP.2019.2891707

These mantle cloaks are designed to produce an “antiphase” scattering currents to cancel the scattering from radiator alone [11]. They can largely suppress cross-band scattering while preserving the performance of the cloaked radiator. In [1] and [13], cloaks are designed for use in simple BSA cases.

In this paper, a different technique is used to minimize scattering in multiband arrays. This method relies on modifying the LB radiator itself by introducing chokes which effectively divide the conductors of the LB elements into short sections. These sections are significantly shorter than a resonant length at the HB and so have much reduced currents induced in them. This technique is implemented in the multiband BSA array as a demonstration. Cross-dipole, which is a commonly used configuration for BSA elements as described in [16] and [17], is used as the LB element to demonstrate the effectiveness of the method. Chokes that present open circuits at HB and short circuits at LB are used to bridge a number of cuts in the LB dipole arms, forming an LB element with reduced HB currents but with LB performance largely maintained. Although the inserted chokes change the impedance of the LB element, making matching more difficult, satisfactory impedance matching is obtained using baluns and impedance transformers designed following the guidelines given in our previous work [18], [19]. In the reported research, a section of the dual-band dual-polarized array with chokes was constructed and tested. Simulated and measured results demonstrate that addition of the chokes greatly reduces scattering while retaining stable radiation properties across the two bands. The array in this paper is designed to operate at LB ranging from 820 to 1000 MHz and HB from 1710 to 2280 MHz—which cover the operating frequencies of most mobile communication systems, including code division multiple access, Global System for Mobile Communications, Personal Communications Service, and Universal Mobile Telecommunications System. Future work will concentrate on broadening the bandwidth to cover the full 4G bands.

This paper is arranged as follows. Section II demonstrates the scattering problem in the dual-band dual-polarized BSA array section by examining the HB pattern distortion caused by a simple interleaved LB element. Section III discusses the operating principle and the design procedure of the choked LB element. The HB pattern with choked LB element is presented to demonstrate that choking LB arms can suppress the HB scattering effectively. The matching capability and the radiation performance of the choked LB element are also presented to verify that choking LB arms does not degrade its original performance. Section IV presents the simulated and measured results of the dual-band dual-polarized antenna array with choked LB element.

## II. PROBLEM STATEMENT

To begin with, a section of the interleaved dual-band BSA array shown in Fig. 2 using unaltered LB elements is simulated to demonstrate the scattering problem. The complete BSA array consists of array sections repeated in the  $y$ -direction. In this array, a strip-shaped cross-dipole is used as the unaltered LB element, and square-shaped cross-dipoles are used

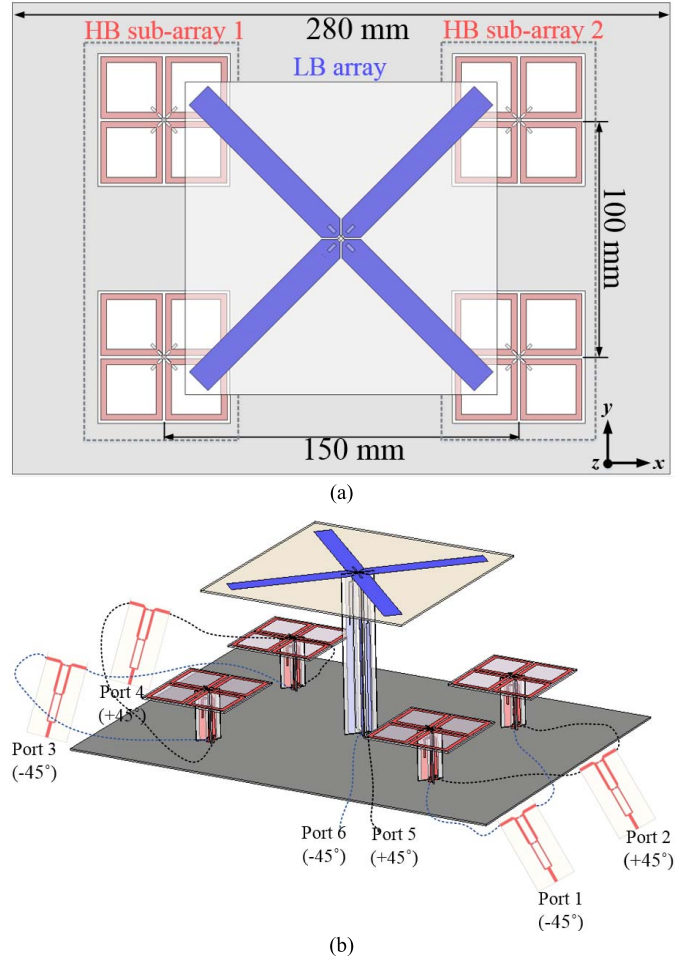


Fig. 2. Configuration of the interleaved BSA array section. (a) Top view. (b) Perspective view.

as the HB elements. Baluns are used to provide balanced feeding and impedance matching for these elements. The LB element is located midway between the four HB elements in two columns. The two HB columns form two HB sub-arrays, and they are fed from independent wideband phase-shifters which for modeling purposes are represented as power dividers, as shown in Fig. 2(b). HB elements with the same polarizations in one column are excited simultaneously. The LB element is fed separately at the inputs to the two baluns. The parameters for the array arrangement are marked in Fig. 2. Those parameters were chosen for good MIMO performance while keeping the array compact. The S-parameters for the LB and HB elements when alone are shown in Fig. 3. The LB element operates from 0.82 to 0.98 GHz, and the HB element operates from 1.70 to 2.30 GHz.

It is apparent from Fig. 2(a) that the LB element overlaps the HB elements. The close spacing between LB and HB elements causes scattering of HB signal by the LB element. The simulated current distribution in the array with unaltered LB element at 1.7 GHz is shown in Fig. 4. Most of the induced current on the LB arms has the same direction as the HB driven current. These currents reradiate, resulting in a deteriorated HB radiation pattern. The radiation patterns in the horizontal plane ( $xoz$  plane) with and without the LB element are shown in Fig. 5 at 1.7, 1.8, and 1.9 GHz.

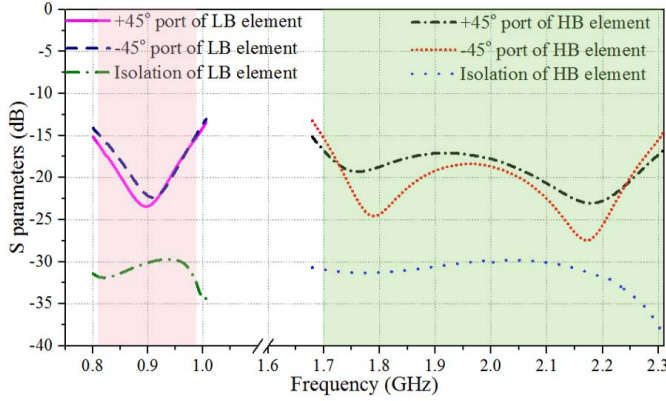


Fig. 3. Simulated S-parameters for the LB and HB antennas when working alone.

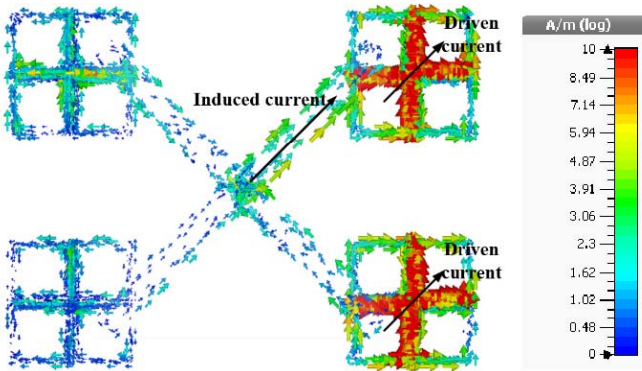


Fig. 4. Current distribution on the array section when HB array on the right column is excited at 1.7 GHz.

Without the LB element, the HB array has a symmetrical pattern with main beam pointing at boresight. After the LB element is added, the HB radiation pattern deteriorates, i.e., the main beam splits or shifts away from boresight. In the worst case, the main lobe direction of the pattern is tilted to  $19^\circ$ , as shown in Fig. 5(a). The distorted radiation patterns obtained after adding the LB element cannot provide the required coverage, and lead to signal loss in particular areas. This is generally unacceptable by cellular operators. It is therefore very desirable to find a method of suppressing the scattering and restoring the pattern in such multiband BSAs.

### III. DESIGN OF CHOKED LOW-BAND ELEMENT

To minimize the scattering shown earlier, one effective way is to suppress the induced HB currents on the LB arms. In this paper, this is achieved by introducing chokes periodically along LB dipole arms to block the HB currents but affect LB currents as little as possible, as shown in Fig. 6. These chokes should present an open circuit at HB and a short circuit at LB. The design principle and the performance of the choked LB antenna are detailed in the following.

#### A. Circuit Model of the Choke

The circuit model of the choke is shown in Fig. 7. It consists of a parallel resonant at HB comprising  $L_1$  and  $C_1$ , and a series

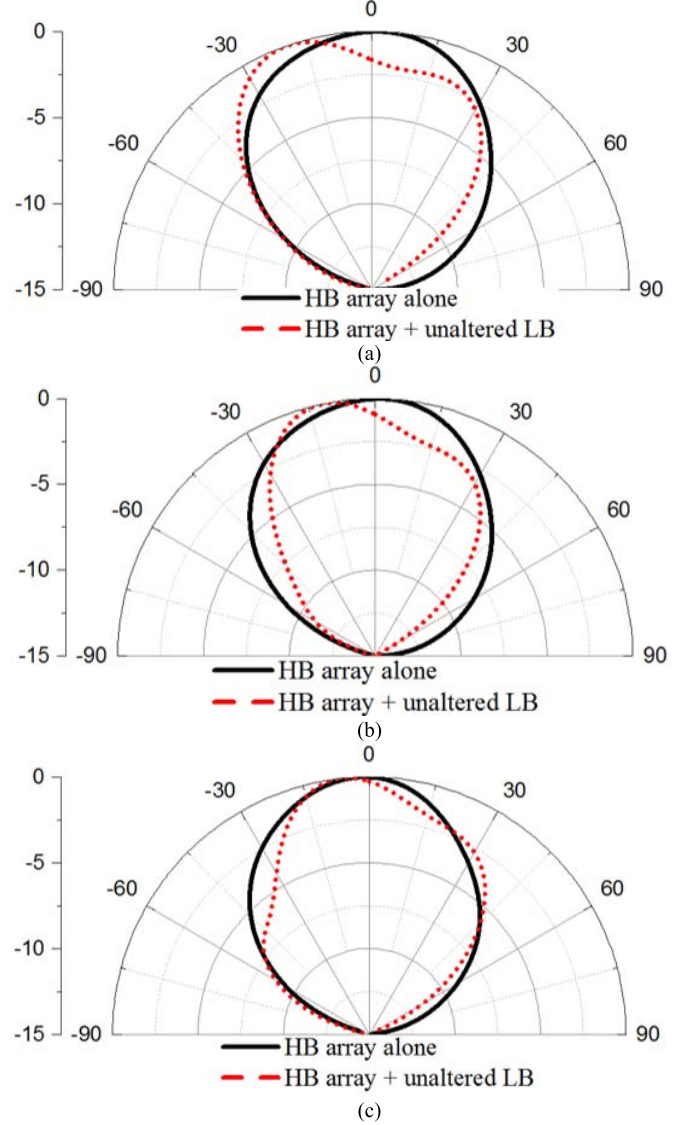


Fig. 5. Horizontal radiation patterns of the HB array: 1) without and 2) with the unaltered LB element at (a) 1.7 GHz, (b) 1.8 GHz, and (c) 1.9 GHz.

resonance at LB with two additional capacitances  $C_2$ . These requirements give

$$j2\pi f_h C_1 + \frac{1}{j2\pi f_h L_1} = 0 \quad (1)$$

$$\frac{2}{j2\pi f_l C_2} + \frac{1}{j2\pi f_l C_1 + \frac{1}{j2\pi f_l L_1}} = 0 \quad (2)$$

where  $f_h$  is the open-circuit frequency point at HB and  $f_l$  is the short-circuit frequency point at LB. The values of  $f_h$  and  $f_l$  are both known in our target application. A remaining variable can be chosen to determine values for all the components  $L_1$ ,  $C_1$ , and  $C_2$

$$Z_c = \sqrt{\frac{L_1}{C_1}}. \quad (3)$$

This equation sets the impedance level at which the choke operates and determines the bandwidths over which the open circuit and short circuit are effective.  $L_1$ ,  $C_1$ , and  $C_2$  can be

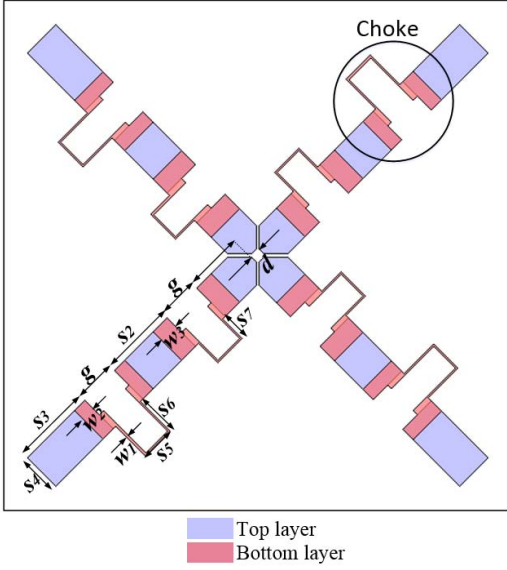


Fig. 6. Configuration of the choked radiator.

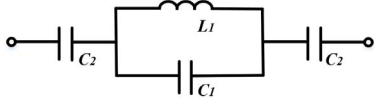


Fig. 7. Circuit model of the choke.

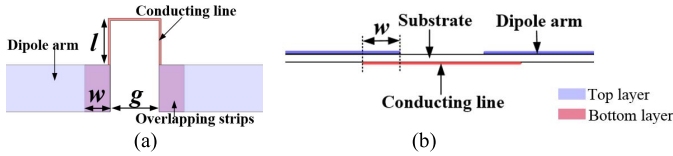


Fig. 8. (a) Top and (b) side views of the realized choke.

found given  $f_h$ ,  $f_l$ , and  $Z_c$ . By suitably choosing  $L_1$ ,  $C_1$ , and  $C_2$ , we can attain desired open-circuit and short-circuit frequency points at HB and LB, respectively.

### B. Physical Realization of the Choke

The choke circuit is realized by a conducting strip structure, as shown in Fig. 8(a) and (b). The thin conducting strip and the capacitance across the gap in the dipole arm provide  $L_1$  and  $C_1$ .  $C_2$  is realized by placing the inductive lines on the bottom layer of the substrate and adding strips that overlap with dipole arms on the top layer. Therefore, the thin inductive line and gap capacitance control the open circuit at HB, and the overlapping strips control the short circuit at LB. In this way, a geometry that approximately represents the circuit in Fig. 7 is designed. The choke is optimized the following two criteria, i.e., to suppress the current at HB and to create a passband at LB, which are discussed in Sections III-B1 and III-B2, respectively. The number of the chokes to be inserted in the dipole arms is determined in the last step, which is given in Section III-B3. The details of the optimization and analysis are as follows.

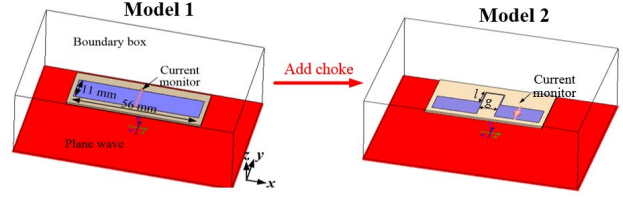


Fig. 9. (a) Model 1: a strip with a length of around  $\lambda/2$  at 2.0 GHz (middle frequency at HB) and a width of 11 mm; Model 2: the strip in Model 1 cut in the middle and bridged with an inductive line. (b) Comparison of induced HB current on the strip in Model 1, and on the strip in Model 2 with a different value of  $l$ . (c) Comparison of induced HB current on the strip in Model 1, and on the strip in Model 2 with different value of  $g$ . (d) Comparison of induced HB currents on the strip in Model 2 with optimized  $\{g, l\}$  values for open-circuit point at 2.0 GHz.

1) *Optimization of the Choke for HB suppression:* First, the choke is optimized to suppress an induced current at HB around 2.0 GHz. To assess the effect of the choke suppressing scattering, it is introduced into a strip representing a section of the dipole arm with a length around  $\lambda/2$  at 2.0 GHz, as shown in Fig. 9(a) ( $\lambda/2$  is the resonant length including the effects of strip width and the dielectric of the substrate). Model 1 shows the strip without modification, and Model 2 shows a gap of

width  $g$  introduced at the center of the strip. An inductive line of length of  $2l + g$  is used to bridge the cut. This inductive line and the gap capacitance are used to realize  $C_1$  and  $L_1$  in the choke equivalent circuit. Guided by the circuit, adjusting  $g$  and  $l$  can effectively tune the open-circuit frequency point.

The models are illuminated by a plane wave with  $E$ -field parallel to the length of the strip, and the maximum induced HB currents flowing on the strips are monitored. For Model 1, there is a noticeable amount of HB current induced on the strip, and the induced current has its peak at around 2.0 GHz, as shown in Fig. 9(b). For Model 2, the maximum induced HB currents with different values of  $g$  and  $l$  are monitored. The results are plotted in Fig. 9(b) and (c). Both figures depict that Model 2 has much less amount of HB current induced on the strips than Model 1, which presents the scattering suppression capability of the choke.

The influences of parameters  $g$  and  $l$  are studied. As shown in Fig. 9(b), for a given  $g$ , increasing  $l$  makes the minimum induced current point to appear at a lower frequency, showing that the open-circuit point is moved to a lower frequency. This is because increasing  $l$  increases  $L_1$ , making  $f_h$  lower. As shown in Fig. 9(c), for a given  $l$ , increasing  $g$  reduces  $C_1$  and moves the open-circuit point slightly to a higher frequency. To achieve open-circuit conditions at 2.0 GHz, different combinations of  $g$  and  $l$  can be chosen. The maximum magnitudes of current flowing on the strip with some suitable combinations are plotted in Fig. 9(d). It shows that combination with larger  $g$  provides current suppression across a wider bandwidth. This is because increasing  $g$  increases  $Z_c$  in (3) and widens the bandwidth of the suppression.

*2) Optimization of the Choke for LB Pass:* After determining parameters  $\{g, l\}$  having desirable scattering suppression at HB, the next step is to optimize the choke to minimize its influence at the operating LB around 0.89 GHz. In this step, a strip with a length of around  $\lambda/2$  at 0.89 GHz is modeled with a choke at the center, as shown in Fig. 10(a). The inductive line is now placed on the bottom layer of the substrate and attached to two patches overlapping the cut segments on the top layer. The overlap width  $w$  determines  $C_2$  in the choke circuit. Adjusting it tunes the short-circuit frequency point.

The models are illuminated by a plane wave at LB, and the maximum induced LB current is monitored. The results are shown in Fig. 10(b). For Model 3, the induced LB current has a peak value at 0.89 GHz. As for Model 4, similar amount of LB current is induced on the strip, but the frequency of the current maximum depends on the value of  $w$ . The frequency of the current maximum corresponds to the short-circuit point. Increasing  $w$  increases  $C_2$  in the circuit, thus moves the short-circuit point to a lower frequency. Therefore, for a given  $\{g, l\}$ , larger  $w$  moves the current maximum to a lower frequency in the simulation, which is shown in Fig. 10(b).

For different combinations of  $\{g, l\}$  that can achieve open-circuit at 2.0 GHz, different values of  $w$  are required to achieve short-circuit point at 0.89 GHz. The induced LB current on the strip of Model 4 with some optimized combinations of  $\{g, l, w\}$  is shown in Fig. 10(c). Combination with larger  $g$  has a narrower bandwidth at LB as they require a smaller value of  $C_2$ . Therefore, the combination of  $\{g, l, w\}$  needs to be

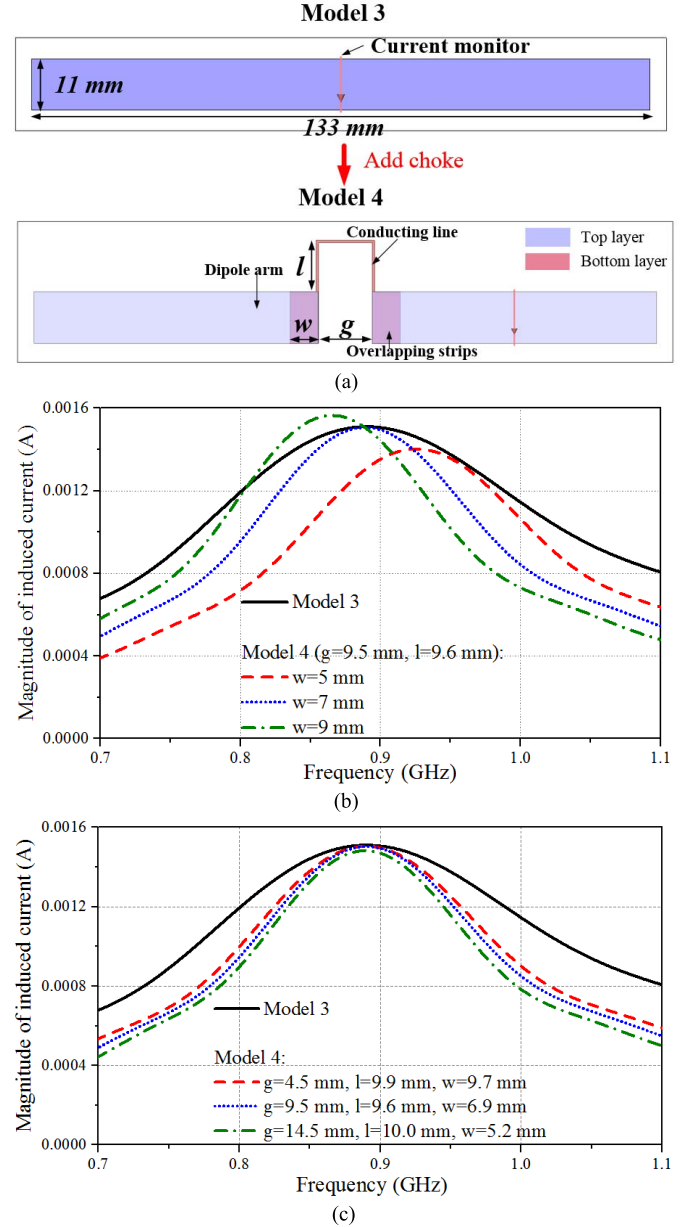
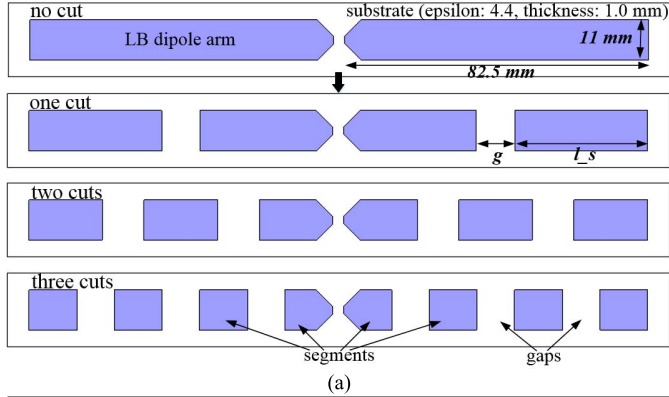


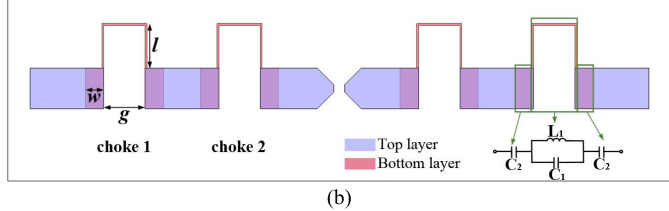
Fig. 10. (a) Model 3: a strip with a length of around  $\lambda/2$  at 0.89 GHz (middle frequency at LB) and a width of 11 mm; Model 4: the strip in Model 3 cut in the middle and bridged with a choke. (b) Comparison of induced LB current on the strip in Model 3, and on the strip in Model 4 with different values of  $w$ . (c) Induced LB current on the strip in Model 4 with optimized  $\{g, l, w\}$  values for open-circuit point at 2.0 GHz and short-circuit point at 0.89 GHz.

selected carefully to achieve the desired passband at LB, and stopband at HB.

*3) Determination of the Number of Chokes Required in the LB Arms:* The LB dipole arms are cut into several short segments with gaps between them, and the chokes described earlier are introduced into the gaps, as illustrated in Fig. 11. It is necessary to determine the number of chokes required in a dipole arm. The choke inevitably introduces some loss to the LB antenna, i.e., the magnitude of the current on a choke is slightly smaller than that on an unmodified strip as shown in Fig. 10(c). Therefore, unnecessary chokes should

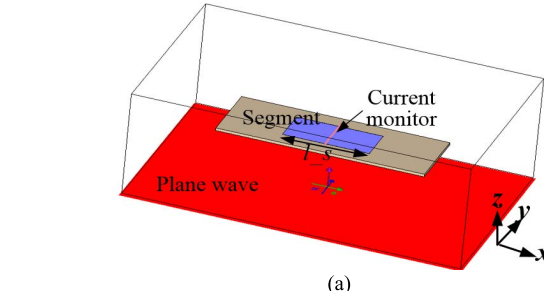


(a)



(b)

Fig. 11. (a) LB dipole arms with a different number of cuts. (b) Top view of the LB dipole arm with chokes inserted.



(a)

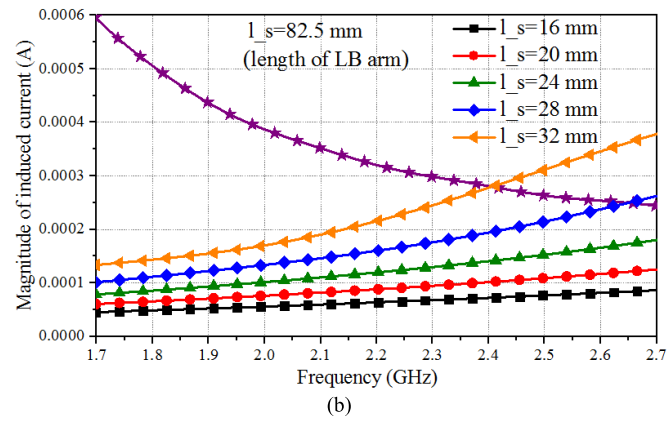


Fig. 12. (a) Model to determine effect of segment length  $l_s$  in free space illuminated by HB plane wave. (b) Maximum induced HB current on the segment with different  $l_s$ .

be avoided. On the other hand, using too few chokes reduces the level of current suppression at HB.

To determine the length of each segment ( $l_s$ ), which assures suitably low HB currents on the segment, segments with different lengths are modeled with illumination by a plane wave with  $E$ -field parallel to the length of the segment, as shown in Fig. 12(a). The maximum induced HB current levels are monitored with results shown in Fig. 12(b). As expected,

TABLE I  
OPTIMIZED PARAMETERS OF THE CHOKED ANTENNA

Parameters	Values (mm)	Parameters	Values (mm)
$s1$	16.75	$s2$	20.5
$s3$	22.25	$s4$	11
$s5$	9.5	$s6$	11
$s7$	7	$g$	11.5
$d$	3	$w1$	0.5
$w2$	4	$w3$	5.5

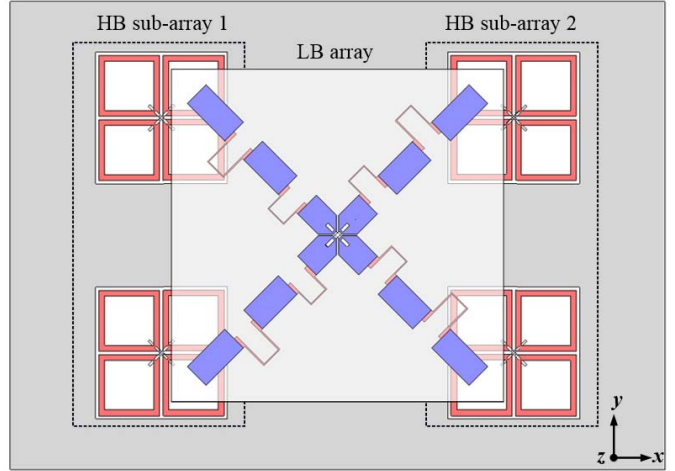


Fig. 13. Arrangement of the interleaved dual-band array with choked LB radiators.

the shorter the segment is the lower the induced current is. Segment lengths around 20 mm offer a great reduction of the HB induced current. For the LB arms, two cuts with a gap width around 11 mm in each arm achieve that. Simulations confirm that the HB radiation pattern is almost unchanged with the cut LB arms.

### C. Scattering Suppression of the Choked LB Radiators

The optimized choked LB radiators are shown in Fig. 6. To achieve HB choking performance across a wideband, two chokes tuned to slightly different frequencies were chosen and introduced into the two gaps in each LB arm. The choked LB arms are still arranged in the cross-dipole configuration to realize the required dual-polarization radiation. The optimized parameters are listed in Table I. The substrate for the radiator has a dielectric constant of 4.4, a loss tangent of 0.0025, and a thickness of 1.0 mm. As the size of the choke in this design is relatively large, the orientation of the chokes is arranged in an anticlockwise direction to minimize coupling between inductors on different arms. If chokes were realized with a smaller dimension, their orientation would be of no consequence.

The optimized choked LB radiators are introduced into the dual-band antenna array as shown in Fig. 13 to examine their effectiveness in suppressing the HB scattering in a realistic environment. Except for the modification of the LB arms,

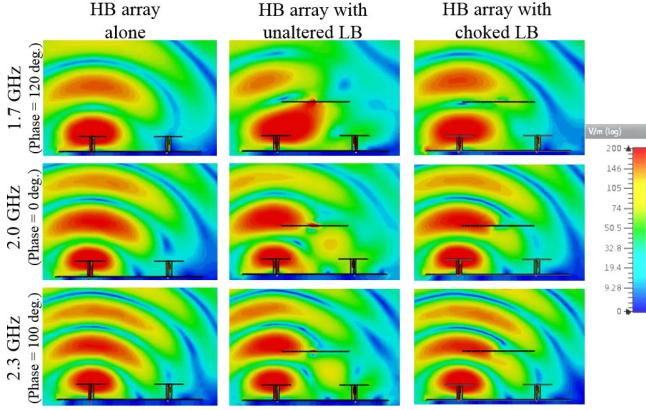


Fig. 14. E-field cuts in the  $xoz$  plane at 1.7, 2.0, and 2.3 GHz under the circumstances of: 1) only HB array; 2) HB array with unaltered LB radiators; and 3) HB array with choked LB radiators.

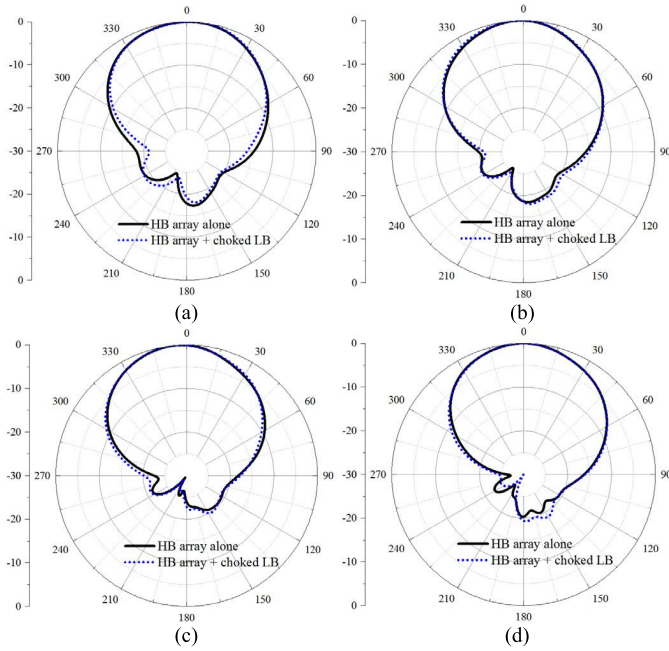


Fig. 15. Comparison of HB radiation patterns under the circumstances of: 1) only HB array and 2) HB array with choked LB radiators at (a) 1.7 GHz, (b) 1.9 GHz, (c) 2.1 GHz, and (d) 2.3 GHz.

the arrangement of this array is unchanged from that shown in Fig. 2. HB elements in one column form one HB subarray and elements with the same polarizations in one subarray are excited simultaneously using wideband power dividers. One column of choked LB elements is located midway between the two HB subarrays, forming an interleaved dual-band dual-polarized BSA array.

Fig. 14 shows the plots of  $E$ -field in a horizontal section through the array across the HB in the cases: 1) HB array only; 2) HB array with unaltered LB radiators; and 3) HB array with choked LB radiators. It is clear that the unaltered LB radiators block HB electric field to a large extent, especially at low frequencies. The proposed choked LB radiators have much less effect on the field than the unaltered LB radiators. The resultant horizontal HB patterns after adding the choked

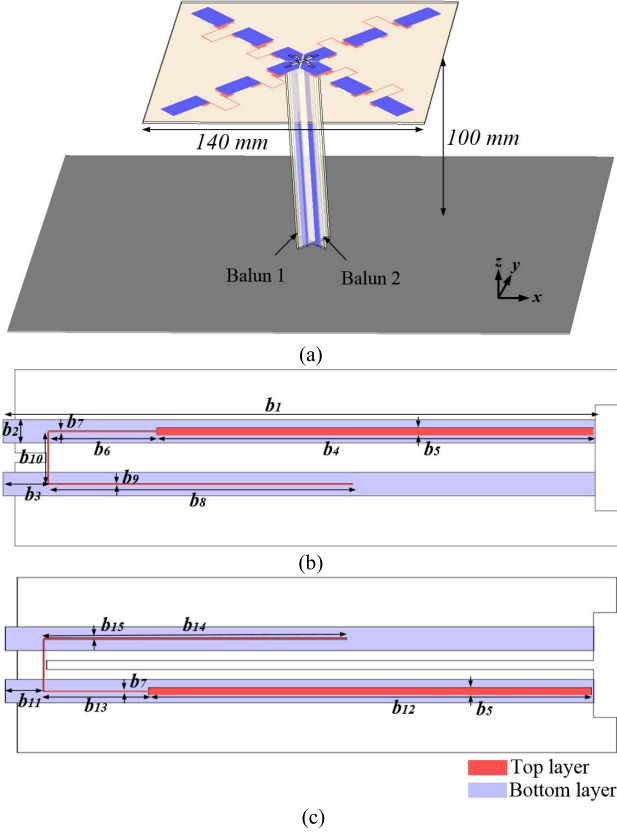


Fig. 16. (a) Perspective view of the choked LB antenna. Configurations of (b) balun 1 and (c) balun 2 (the baluns are printed on both sides of a substrate with a dielectric constant of 4.4, a loss tangent of 0.0025, and a thickness of 1.5 mm).

TABLE II  
OPTIMIZED PARAMETERS OF BALUNS FOR THE CHOKED ANTENNA

Parameters	Values (mm)	Parameters	Values (mm)
$b_1$	101	$b_2$	4
$b_3$	7.6	$b_4$	72.98
$b_5$	1.4	$b_6$	20
$b_7$	0.2	$b_8$	50
$b_9$	0.2	$b_{10}$	9
$b_{11}$	6.475	$b_{12}$	74.08
$b_{13}$	20	$b_{14}$	50
$b_{15}$	0.25		

LB radiators are shown in Fig. 15. Patterns for HB array alone are added for comparison. It is observed that the HB radiation patterns in the presence of choked LB radiators are almost the same as those of HB array alone, demonstrating the effectiveness of the chokes in reducing the HB pattern distortion across the band.

#### D. Performance of the Choked LB Element

As the realized chokes are not ideal and can only approximate a short circuit over a limited range of LB frequencies,

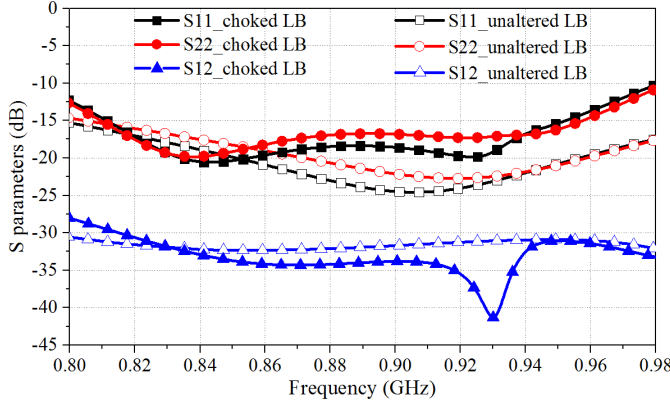


Fig. 17. S-parameters of the choked LB element and the unaltered LB element.

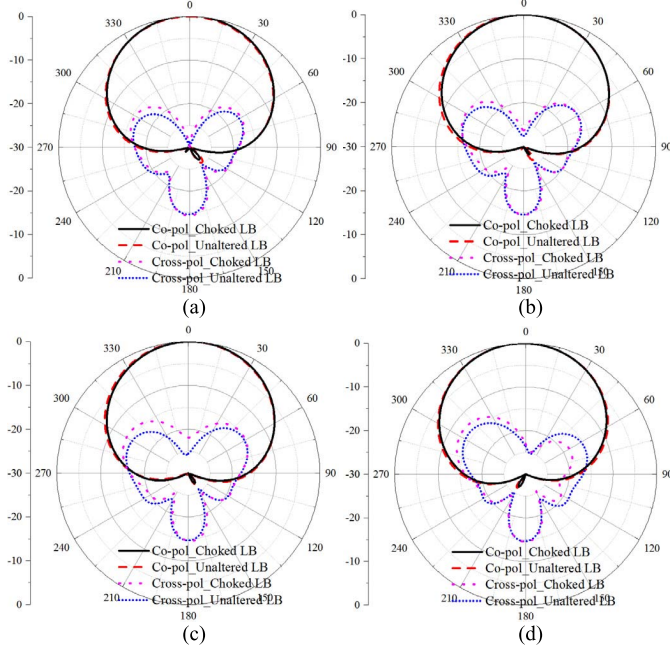


Fig. 18. Radiation patterns of the choked LB element and the unaltered LB element at (a) 0.82 GHz, (b) 0.88 GHz, (c) 0.92 GHz, and (d) 0.96 GHz.

they can change the impedance properties of the LB element, making the impedance matching task more difficult. Nevertheless, following the guidelines of designing the impedance matching network given in [18] and [19], a satisfactory matching result is obtained using baluns and impedance matching elements. Two baluns are orthogonally arranged to feed the two pairs of choked dipoles. The configurations of the choked LB element together with the two baluns are shown in Fig. 16. The detailed parameters of the baluns are listed in Table II. Fig. 17 shows the matching results for the choked element. The antenna is matched to reflection coefficients  $< -14$  dB from 0.82 to 0.96 GHz. Compared with the unaltered LB element, the matching of the choked LB element is slightly degraded, but it is still satisfactory. The simulated radiation patterns of LB element with choked arms and unaltered arms at 0.82, 0.88, 0.92, and 0.96 GHz are shown in Fig. 18. The patterns in the two cases are almost identical, showing that choking LB arms does not influence the radiation performance.

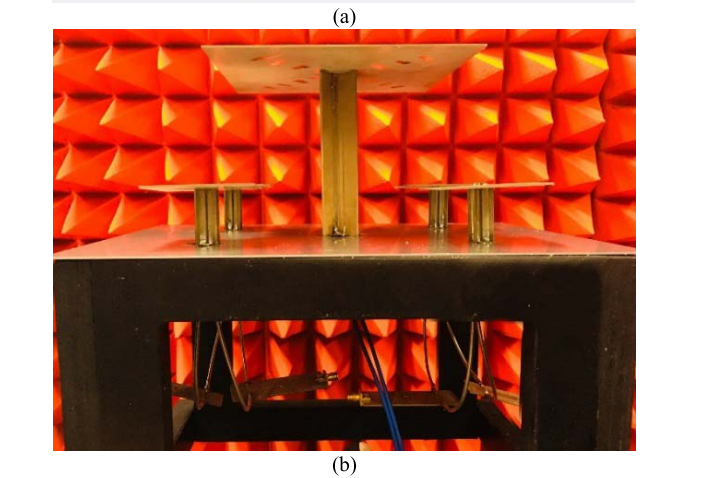
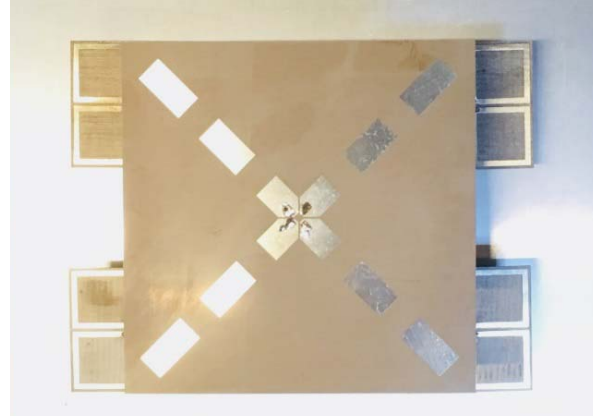


Fig. 19. (a) Top and (b) side views of the dual-band dual-polarized interleaved array.

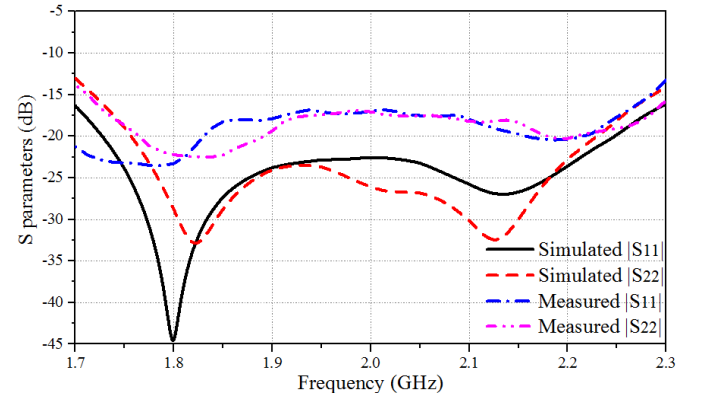


Fig. 20. Simulated and measured reflection coefficients of the HB array.

#### IV. SIMULATED AND MEASURED RESULTS OF THE DUAL-BAND DUAL-POLARIZED ARRAY USING THE CHOKE ELEMENT

The prototype of the antenna array section was fabricated and tested, as shown in Fig. 19. Fig. 20 shows the simulated and measured reflection coefficients of the HB array. The results for the two HB arrays in the two columns are essentially the same due to the symmetric structure, so only the results for one column of the HB array are given. The HB reflection coefficients as expected are almost the same as obtained without the LB elements. Measured results agree well with

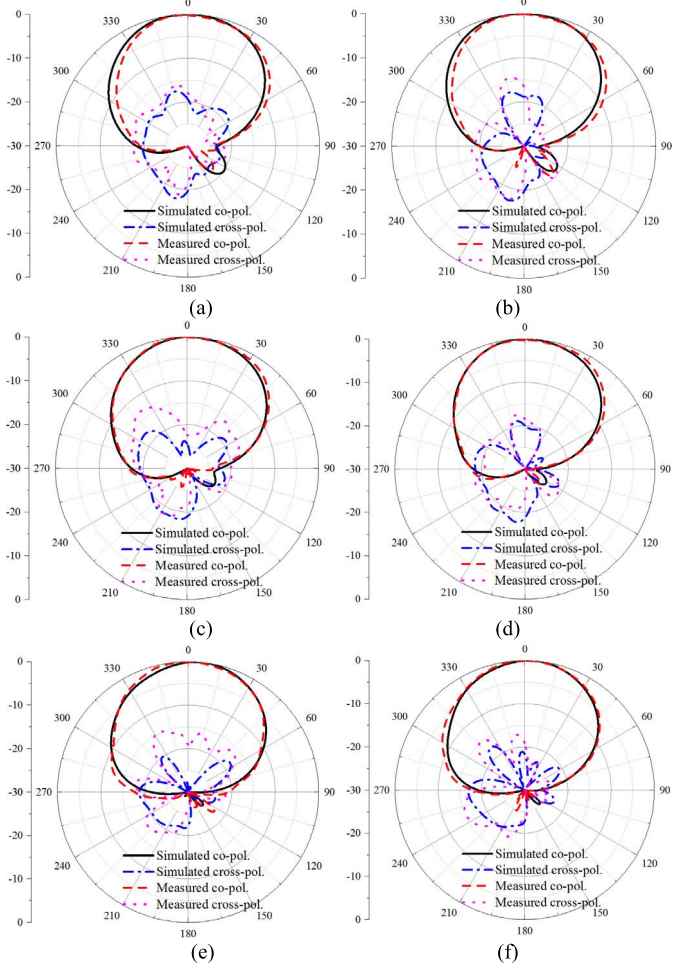


Fig. 21. Simulated and measured radiation patterns of the HB array. (a) Port 1 at 1.7 GHz. (b) Port 2 at 1.7 GHz. (c) Port 1 at 1.9 GHz. (d) Port 2 at 1.9 GHz. (e) Port 1 at 2.2 GHz. (f) Port 2 at 2.2 GHz.

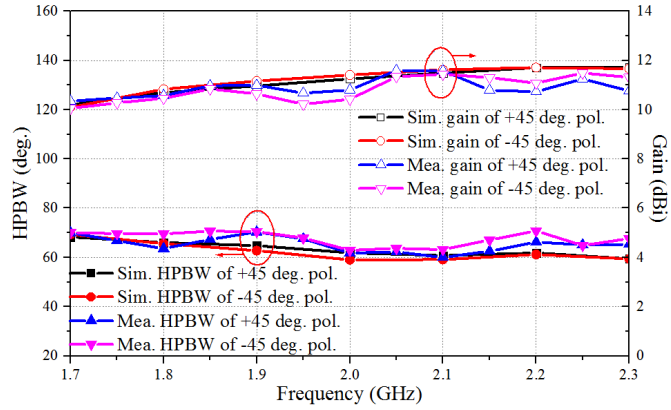


Fig. 22. Simulated and measured horizontal HPBW and realized gain of the HB array.

the simulated ones, demonstrating a good matching across a band of 28.6% from 1.71 to 2.28 GHz. The radiation patterns for the  $\pm 45^\circ$  polarization in one column at 1.7, 1.9, and 2.2 GHz are shown in Fig. 21. The simulated and measured patterns agree well. The simulated and measured cross polarization discriminations (XPDs) at the boresight are  $>19$  and  $>16$  dB, respectively. Fig. 22 shows the simulated

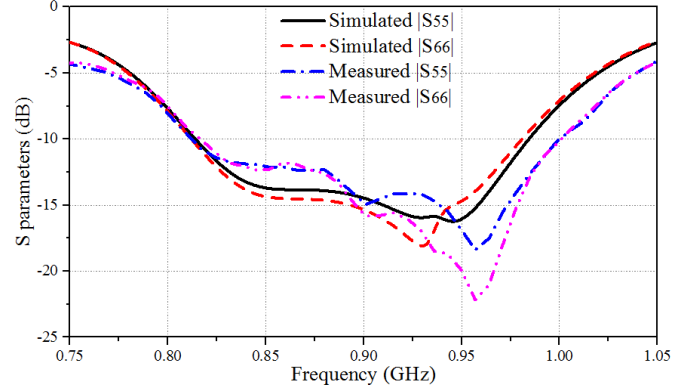


Fig. 23. Simulated and measured S-parameters of the choked LB antenna.

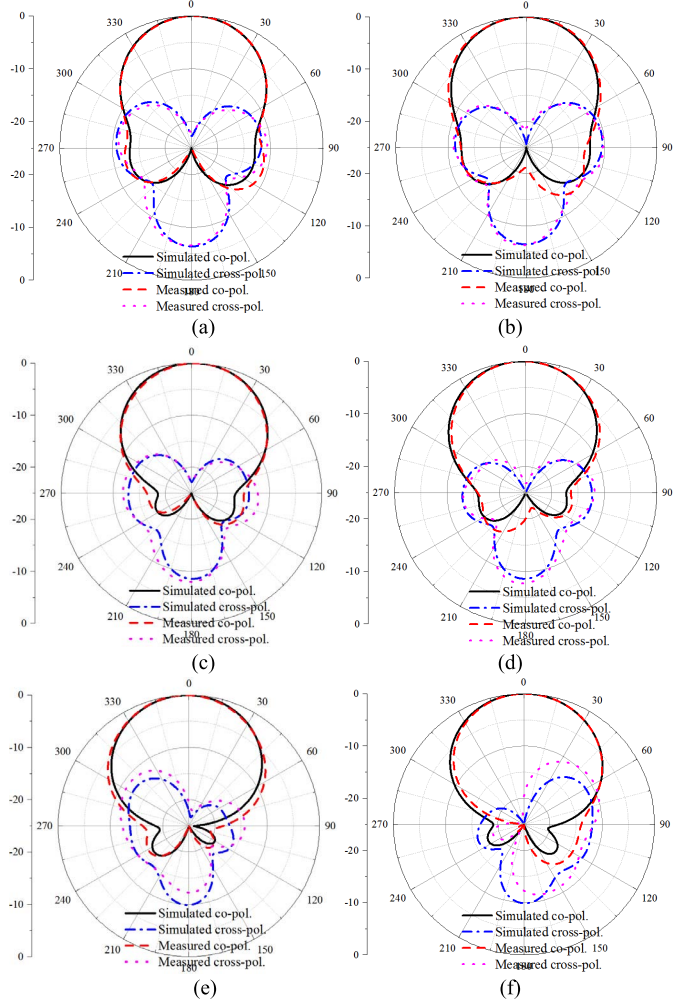


Fig. 24. Simulated and measured radiation pattern of the choked LB antenna. (a) Port 1 at 0.82 GHz. (b) Port 2 at 0.82 GHz. (c) Port 1 at 0.88 GHz. (d) Port 2 at 0.88 GHz. (e) Port 1 at 0.96 GHz. (f) Port 2 at 0.96 GHz.

and measured horizontal half-power beamwidths (HPBWs) and the realized gain of the HB array. For each polarization, the measured HPBW varies within  $65^\circ \pm 5^\circ$ , which shows that the array has very stable radiation performance as required in base station applications. The simulated and measured realized gains both vary from 10 to 12 dBi. All the four HB ports have efficiencies higher than 90% across the operating band.

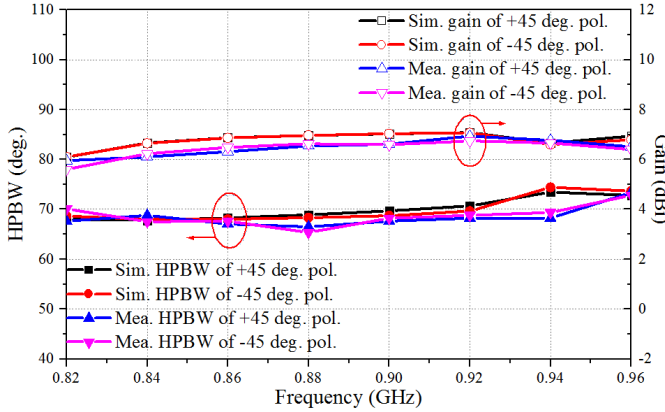


Fig. 25. Simulated and measured HPBW and realized gain of the choked LB antenna.

The performance of HB array with choked LB is almost the same as that of HB array only. The simulated and measured choked LB antenna results are shown in Figs. 23–25. As shown in Fig. 23, the measured bandwidth is 19.7% from 0.82 to 1.0 GHz for reflection coefficients  $< -10$  dB. The simulated and measured horizontal radiation patterns of the choked LB antenna at 0.82, 0.88, and 0.96 GHz are shown in Fig. 24. The simulated and measured radiation patterns agree well. The measured XPD is  $>20$  dB at boresight. The horizontal HPBW and realized gain are shown in Fig. 25. The simulated and measured HPBWs vary within  $71.5^\circ \pm 3.5^\circ$  and  $69.5^\circ \pm 4^\circ$ , respectively. The measured gain varies from 6.0 to 7.0 dBi, which is slightly less than the simulated one. It is mainly caused by the loss of cables. The efficiencies of the LB antenna are higher than 89% across the band. Note that the presented gain results for HB and LB antennas are only for one array section. Higher gain can be obtained by repeating the array sections in the vertical direction ( $y$ -direction).

## V. CONCLUSION

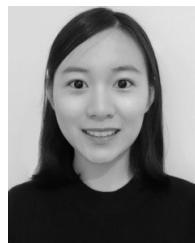
In this paper, a method of suppressing cross-band scattering by choking the LB elements in an interleaved multiband antenna array is presented. The technique is demonstrated and analyzed in the context of a dual-band dual-polarized interleaved base station array configuration covering bands of 0.82–1.0 GHz and 1.71–2.28 GHz. Simulated and measured results both demonstrate that choking the LB element largely restores the HB radiation pattern. The chokes have some effects on the LB impedance characteristics but satisfactory performance can still be obtained with a suitable choice of choke impedances and optimized feed networks. The realized array section has stable radiation patterns in both the HB and LB with a compact size. Similar choking methods can be adopted to solve cross-band scattering issue in other multiband antenna systems.

## ACKNOWLEDGMENT

The authors would like to thank Z. Li with Beijing Jiaotong University for his valuable suggestions on this paper.

## REFERENCES

- [1] J. C. Soric, A. Monti, A. Toscano, F. Bilotti, and A. Alù, “Dual-polarized reduction of dipole antenna blockage using mantle cloaks,” *IEEE Trans. Antennas Propag.*, vol. 63, no. 11, pp. 4827–4834, Nov. 2015.
- [2] Y. He, Z. Pan, X. Cheng, Y. He, J. Qiao, and M. M. Tentzeris, “A novel dual-band, dual-polarized, miniaturized and low-profile base station antenna,” *IEEE Trans. Antennas Propag.*, vol. 63, no. 12, pp. 5399–5408, Dec. 2015.
- [3] H. Huang, Y. Liu, and S. Gong, “A novel dual-broadband and dual-polarized antenna for 2G/3G/LTE base stations,” *IEEE Trans. Antennas Propag.*, vol. 64, no. 9, pp. 4113–4118, Sep. 2016.
- [4] H. Huang, Y. Liu, and S. Gong, “A dual-broadband, dual-polarized base station antenna for 2G/3G/4G applications,” *IEEE Antennas Wireless Propag. Lett.*, vol. 16, pp. 1111–1114, 2017.
- [5] G. Cui, S.-G. Zhou, G. Zhao, and S.-X. Gong, “A compact dual-band dual-polarized antenna for base station application,” *Prog. Electromagn. Res. C*, vol. 64, pp. 61–70, 2016.
- [6] Y. He, W. Tian, and L. Zhang, “A novel dual-broadband dual-polarized electrical dumbbell base station antenna for 2G/3G applications,” *IEEE Access*, vol. 5, pp. 15241–15249, 2017.
- [7] Y. Liu, S. Wang, N. Li, J.-B. Wang, and J. Zhao, “A compact dual-band dual-polarized antenna with filtering structures for sub-6 GHz base station applications,” *IEEE Antennas Wireless Propag. Lett.*, vol. 17, no. 10, pp. 1764–1768, Oct. 2018.
- [8] Y.-B. Jung and S.-Y. Eom, “A compact multiband and dual-polarized mobile base-station antenna using optimal array structure,” *Int. J. Antennas Propag.*, vol. 2015, 2015, Art. no. 178245.
- [9] L. Y. Nie *et al.*, “A low-profile coplanar dual-polarized and dual-band base station antenna array,” *IEEE Trans. Antennas Propag.*, vol. 66, no. 12, pp. 6921–6929, Dec. 2018.
- [10] B. B. Jones, O. Isik, and C. Shang, “Dual-band interspersed cellular basestation antennas,” EP Patent 2769476 B1, Dec. 24, 2012.
- [11] A. Monti, J. Soric, A. Alù, F. Bilotti, A. Toscano, and L. Vigni, “Overcoming mutual blockage between neighboring dipole antennas using a low-profile patterned metasurface,” *IEEE Antennas Wireless Propag. Lett.*, vol. 11, pp. 1414–1417, 2012.
- [12] Z. H. Jiang, P. E. Sieber, L. Kang, and D. H. Werner, “Restoring intrinsic properties of electromagnetic radiators using ultralightweight integrated metasurface cloaks,” *Adv. Funct. Mater.*, vol. 25, no. 29, pp. 4708–4716, Aug. 2015.
- [13] A. Monti *et al.*, “Mantle cloaking for co-site radio-frequency antennas,” *Appl. Phys. Lett.*, vol. 108, no. 11, p. 113502, 2016.
- [14] H. M. Bernety and A. B. Yakovlev, “Reduction of mutual coupling between neighboring strip dipole antennas using confocal elliptical metasurface cloaks,” *IEEE Trans. Antennas Propag.*, vol. 63, no. 4, pp. 1554–1563, Apr. 2015.
- [15] S. Vellucci, A. Monti, M. Barbuto, A. Toscano, and F. Bilotti, “Satellite applications of electromagnetic cloaking,” *IEEE Trans. Antennas Propag.*, vol. 65, no. 9, pp. 4931–4934, Sep. 2017.
- [16] Y. Cui, R. Li, and H. Fu, “A broadband dual-polarized planar antenna for 2G/3G/LTE base stations,” *IEEE Trans. Antennas Propag.*, vol. 62, no. 9, pp. 4836–4840, Sep. 2014.
- [17] C. Ding, H. Sun, R. W. Ziolkowski, and Y. J. Guo, “Simplified tightly-coupled cross-dipole arrangement for base station applications,” *IEEE Access*, vol. 5, pp. 27491–27503, 2017.
- [18] H. Sun, C. Ding, B. Jones, and Y. J. Guo, “A wideband base station antenna element with stable radiation pattern and reduced beam squint,” *IEEE Access*, vol. 5, pp. 23022–23031, 2017.
- [19] C. Ding, B. Jones, Y. J. Guo, and P.-Y. Qin, “Wideband matching of full-wavelength dipole with reflector for base station,” *IEEE Trans. Antennas Propag.*, vol. 65, no. 10, pp. 5571–5576, Oct. 2017.



**Hai-Han Sun** (GS’17) was born in Shandong, China, in 1994. She received the bachelor’s degree in electronic information engineering from the Beijing University of Posts and Telecommunications, Beijing, China, in 2015. She is currently pursuing the Ph.D. degree in engineering with the University of Technology Sydney, Sydney, NSW, Australia.

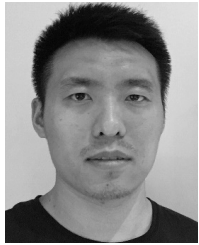
Her current research interests include base station antennas and wideband omnidirectional antennas.



**Can Ding** (M'17) was born in Anhui, China, in 1989. He received the bachelor's degree in microelectronics from Xidian University, Xi'an, China, in 2009, and the Ph.D. degree from Macquarie University, Sydney, NSW, Australia, in 2015.

From 2012 to 2015, he was with Macquarie University, Xidian University, and Commonwealth Scientific and Industrial Research Organisation DPoS Flagship, Marsfield, Australia. From 2015 to 2017, he was a Post-Doctoral Research Fellow with the University of Technology Sydney (UTS),

Sydney, where he is currently a Lecturer with the Global Big Data Technologies Centre. His current research interests include antennas and terahertz fibers.



**He Zhu** (M'18) received the B.Sc. and M.Eng. degrees from the South China University of Technology, Guangzhou, China, and the Ph.D. degree in electrical engineering from the School of ITEE, University of Queensland, Brisbane, QLD, Australia.

He is currently a Post-Doctoral Research Fellow with the Global Big Data Technologies Centre, University of Technology Sydney, Sydney, NSW, Australia. His current research interests include development of beam-forming networks for antenna arrays, radio frequency integrated circuits and systems, and tunable microwave and mm-wave devices.



**Bevan Jones** (LM'13) was born in Sydney, NSW, Australia. He received the B.Sc. and B.E. (Hons.) degrees and the Ph.D. degree in electrical engineering from the University of Sydney, Sydney, in 1967, 1970, and 1974, respectively.

From 1974 to 1977, he was a Post-Doctoral Fellow with Max-Planck-Institut für Radioastronomie, Bonn, Germany, where he was involved in the design of a millimeter wavelength radio telescope. From 1980 to 1982, he led a group of 12 Australian engineers working on this project in the U.S. with a joint venture partner. After two years as a Lecturer at Wollongong University, Wollongong, Australia, he returned to Germany as a Scientist to continue his previous work. He returned to Australia in 1980 to work on the Interscan Project to develop a microwave aircraft landing system (MLS). From 1983 to 1994, he was the Technical Director of Interscan Australia Pty Ltd., Rydalmer, NSW, Australia a research and development company owned and funded by the Australian Industry Development Corporation. From 1992 to 1993, he was involved in the development of early cellular base station antennas, the first with adjustable electrical beam tilt at the time when the original AMPS system was being rolled out. He led the development of many antenna-based products including the MLS, a C-band phased array precision approach system, an electronically scanned TACAN navigation beacon, a large vertical aperture secondary surveillance radar antenna, and an advanced S-band multibeam phased array

primary radar antenna. In 1994, together with two partners, he founded Argus Technologies, Mulgrave, Australia, and served as the Managing Director for ten years and then as the Technical Director. The company has specialized solely in the design and manufacture of cellular base station antennas and expanded its market reach worldwide. The company initially operated in Sydney but set up a second manufacturing facility in Guangzhou, China, in 2001, and later established a research and development capability. Since its inception, Argus Technologies has brought many innovations to market and became a major international supplier of cellular antennas. In 2011, the company was acquired by a U.S. multinational, where he served as the Technical Director under the new ownership for a further two years, during which time he was largely engaged in technical instruction of the group's engineering teams in the U.S. and China. Following that he retired from full-time work, and since then, he has been doing a number of consulting jobs on antenna related topics. He is currently an Adjunct Professor with the University of Technology Sydney (UTS), Sydney. He has authored a number of articles in technical journals. He holds patents relating to antenna components and has done consulting on antennas and electromagnetics for a number of companies including Raytheon and British Aerospace and has taught specialist courses in numerical methods and electromagnetics at universities.



**Y. Jay Guo** (F'14) received the bachelor's and master's degrees from Xidian University, Xi'an, China, in 1982 and 1984, respectively, and the Ph.D. degree from Xian Jiaotong University, Xi'an, in 1987.

He held various senior technology leadership positions at Fujitsu, London, U.K., Siemens, London, and NEC in the U.K. In 2014, he was the Director with Commonwealth Scientific and Industrial Research Organization, Marsfield, NSW, Australia, where he was directing a number of ICT research portfolios. He is currently a Distinguished Professor and the Founding Director of the Global Big Data Technologies Centre, University of Technology Sydney, Sydney, NSW, Australia. He has authored or co-authored over 400 research papers. He holds 24 patents in antennas and wireless systems. His current research interest includes antennas, mm-wave and terahertz communications and sensing systems as well as big data technologies.

Dr. Guo is a fellow of the Australian Academy of Engineering and Technology and IET. He is a member of the College of Experts of Australian Research Council. He was a recipient of a number of the most prestigious Australian national awards, and was named one of the most influential engineers in Australia in 2014 and 2015. He has chaired numerous international conferences. He is the Chair Elect of the International Steering Committee and International Symposium on Antennas and Propagation. He was the International Advisory Committee Chair of IEEE VTC2017, the General Chair of ISAP2015, IWAT2014, and WPMC'2014, and the TPC Chair of 2010 IEEE WCNC and 2012 and 2007 IEEE ISCIT. He served as a Guest Editor for the Special Issues on Antennas for Satellite Communications and Antennas and Propagation Aspects of 60–90 GHz Wireless Communications, both in the IEEE TRANSACTIONS ON ANTENNAS AND PROPAGATION Special Issue on Communications Challenges and Dynamics for Unmanned Autonomous Vehicles, IEEE JOURNAL ON SELECTED AREAS IN COMMUNICATIONS, and the IEEE Network Special Issue on 5G for Mission Critical Machine Communications.